

Vibrational Spectra of Eight-Coordinate Niobium and Tantalum Complexes with Peroxo Ligands: A Theoretical Simulation

Daisy Bayot,^[a] Michel Devillers,^[a] and Daniel Peeters*^[b]

Keywords: Density functional calculations / IR spectroscopy / Niobium / Tantalum / Peroxo ligands / Raman spectroscopy

A theoretical interpretation of the experimental observations made by vibrational IR and Raman spectroscopy on eight-coordinate peroxo complexes of niobium(V) and tantalum(V) is carried out. The theoretical study, realised on stoichiometric models of general formula $[M(O_2)_4]^{3-}$, $[M(O_2)_3L_2]^{x-}$, *cis*- and *trans*- $[M(O_2)_2L_4]^{y-}$ and $[M(O_2)L_6]^{z-}$ ($M = Nb^V$ or Ta^V), provides the normal modes of vibrations involving peroxo li-

gands, their corresponding calculated frequency and their activity in IR and/or Raman spectroscopy. The theoretical results from the model complexes are compared with experimental IR and Raman spectroscopic data.

(© Wiley-VCH Verlag GmbH & Co. KGaA, 69451 Weinheim, Germany, 2005)

Introduction

In the last decades, peroxo species of transition metals have attracted considerable attention because of their extended coordination chemistry as well as their role in several challenging domains. Peroxo species of d^0 transition metals, for example V^V , Ti^{IV} , Mo^{VI} , W^{VI} and Nb^V , are potential oxygen donors to organic substrates in the liquid phase.^[1–5] They can act as stoichiometric oxidants or as catalysts in the presence of oxidizing agents, such as H_2O_2 or $tBuOOH$, that are used to regenerate the starting peroxo metal species in situ. Such peroxo complexes can oxidize some electrophilic species and a large variety of nucleophilic substrates, such as phosphanes, sulfides, alcohols, olefins, enolates, imines, amides, etc.^[3]

A further interest in peroxo complexes results from the important role they play in biological systems. For example, peroxovanadium(V) complexes have been found to have anti-tumour and insulin mimetic activities, while others have been studied as functional models for the vanadium haloperoxidase enzymes.^[6,7] Finally, because such peroxo-type coordination compounds are most of the time soluble in water, they are also of great interest as precursors for the preparation of oxide materials and, more particularly, multimetallic oxides involving highly polarizing d^0 transition metals like Ti^{IV} , Zr^{IV} , Nb^V or Ta^V , for which the availability of water-soluble compounds is very limited.^[8–13] This

“peroxo way” has recently been shown to be a valuable approach for the synthesis of mixed oxides containing niobium and/or tantalum from well-defined and pre-isolated complexes.^[14,15]

The peroxo compounds of transition metals correspond either to homoleptic complexes or to heteroleptic ones. In the heteroleptic compounds, one to three coordinated peroxo groups are associated with one or more monodentate or polydentate ligands. The various ways in which a peroxo group is expected to coordinate to metals are illustrated in Figure 1, but the most common type, observed for d^0 transition metals, is the so-called side-bonded peroxo ligand, complexed in an η^2 mode.

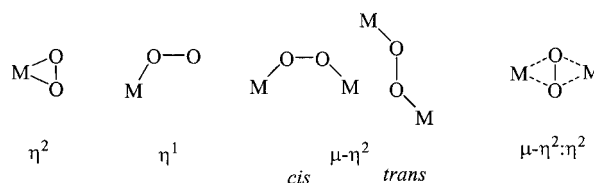


Figure 1. Coordination modes of peroxo groups to metal atoms.

The coordination polyhedra in heteroleptic peroxo compounds are fairly predictable. For the heavy group five elements niobium and tantalum, for example, coordination number 8 with dodecahedral geometry has invariably been observed. Several structural analyses of such heteroleptic complexes have been carried out, revealing the actual coordination spheres in each case.^[14,16–21] However, most of the time no crystal structure could be obtained, and the determination of the metal environment in the complex is ambiguous. In that context, vibrational spectroscopy is still essential to characterise complexes containing coordinated peroxo groups. In the case of side-bonded peroxo ligands, two types of vibrational modes are expected: the peroxo stretch-

[a] Unité de Chimie des Matériaux Inorganiques et Organiques, Université Catholique de Louvain, Place Louis Pasteur 1, 1348 Louvain-la-Neuve, Belgium

[b] Unité de Chimie Structurale et des Mécanismes Réactionnels, Université Catholique de Louvain, Place Louis Pasteur 1, 1348 Louvain-la-Neuve, Belgium
Fax: +32-10-472-707
E-mail: peeters@chim.ucl.ac.be

Supporting information for this article is available on the WWW under <http://www.eurjic.org> or from the author.

ing, $\nu(\text{O}-\text{O})$, and the metal–peroxo stretching, $\nu[\text{M}(\text{O}_2)]$. As far as niobium and tantalum compounds are concerned, the determination of the number of peroxo ligands present around the metal atom in heteroleptic complexes can be deduced from the number of $\nu(\text{O}-\text{O})$ bands, occurring near 850 cm^{-1} , by using an empirical rule which states that the presence of two or three $\nu(\text{O}-\text{O})$ bands in the IR spectrum indicates the formation of a diperoxo or triperoxo complex, respectively.^[22] As far as homoleptic $[\text{M}(\text{O}_2)_4]^{3-}$ ($\text{M} = \text{Nb}^{\text{V}}$ or Ta^{V}) complexes are concerned, one broad or two $\nu(\text{O}-\text{O})$ bands are observed in the IR and two such bands in the Raman spectra.^[23–26] A recent study reported the vibrational spectra of tetraperoxotantalate compounds with several different counterions, $(\text{A}^1)_3[\text{Ta}(\text{O}_2)_4]$ ($\text{A}^1 = \text{K}^+, \text{Rb}^+, \text{Cs}^+$). The authors determined the different vibrational modes of the O–O and Ta–O stretching vibrations from the site-group analysis of the $[\text{Ta}(\text{O}_2)_4]^{3-}$ anion (site group symmetry D_{2d}).^[26]

The present work deals with the theoretical simulation of the experimental observations made by vibrational IR and Raman spectroscopy on eight-coordinate peroxo complexes of niobium(v) and tantalum(v). This study will provide the normal modes of vibrations involving peroxo ligands, their corresponding frequency and their activity in IR and/or Raman spectroscopy and so constitute a guide to interpret experimental spectra. By validating the empirical rules mentioned so far for the interpretation of the vibrational spectra of eight-coordinate peroxo complexes, this work provides important tools to develop the coordination chemistry of such compounds.

Results and Discussion

Theoretical calculations were performed at the DFT level using various functionals for five stoichiometric models corresponding to tetra-, tri-, di- and monoperoxo species, of general formula $[\text{M}(\text{O}_2)_4]^{3-}$, $[\text{M}(\text{O}_2)_3\text{L}_2]^{x-}$, *cis*- and *trans*- $[\text{M}(\text{O}_2)_2\text{L}_4]^{y-}$ and $[\text{M}(\text{O}_2)\text{L}_6]^{z-}$, respectively. The metal, M, chosen for the simulation is niobium(v) and L corresponds to the oxygen atoms of oxalate, which mimics a coordinated atom from one or several mono- or polydentate ligand(s). More details about the methodologies used and the choices made for the computations are explicitly presented in the Computational Details section (Figure 2).

The symmetry obtained after geometry optimisation for the various compounds $[\text{M}(\text{O}_2)_4]^{3-}$, $[\text{M}(\text{O}_2)_3\text{L}_2]^{x-}$, *cis*- or *trans*- $[\text{M}(\text{O}_2)_2\text{L}_4]^{y-}$ and $[\text{M}(\text{O}_2)\text{L}_6]^{z-}$ is D_{2d} , C_{3v} , C_{2v} or D_2 and C_1 , respectively. For the diperoxo species, their relative stability is small and the results depend on the chosen methodology. As mentioned in the Computational Details section, the C_{2v} symmetry (*cis* configuration) is more stable at the Hartree–Fock level but the opposite is the case at the DFT level. More details about those structures are given in the Supporting Information. For each one, a normal mode analysis was realised at the harmonic level in order to obtain vibration frequencies and to identify the normal modes involving the peroxo functions.

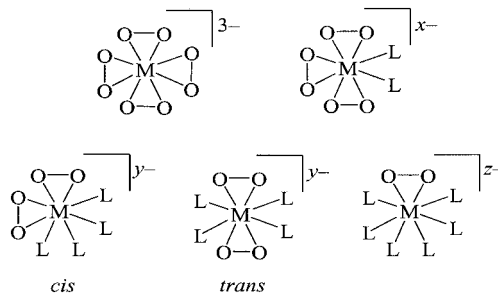


Figure 2. Schematic representation of model stoichiometries considered for the theoretical study ($\text{M} = \text{Nb}^{\text{V}}$ and $\text{L} = \text{oxygen atom from an oxalate ligand}$).

The theoretical values were compared with those of corresponding complexes described in the literature for each of the tetra-, tri- and *cis*-diperoxo species studied. Because the experimental vibrational data of peroxotantalum(v) complexes are quite close to those of their niobium(v) equivalents, some of them are also taken into account in this study and compared to the calculated values. The stoichiometries of the selected representative Nb and Ta complexes are given in Table 1. As far as monoperoxo and *trans*-diperoxo species are concerned, no such compounds with an eight-fold coordination have been described so far in the literature. The IR data from complexes listed in Table 1 have already been reported,^[14,16,17,22,27,28] while little information from Raman spectroscopy is available.

Table 1. Stoichiometries of the peroxo complexes of niobium(v) and tantalum(v) described in the literature and used in this work for comparison (ox = oxalate, *o*-phen = 1,10-phenanthroline, picO = picolinate *N*-oxide, tart = tartrate, edtaO_2 = ethylenediaminetetraacetate *N,N'*-dioxide).

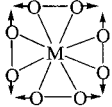
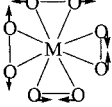

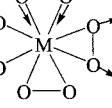
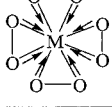
		Stoichiometry	Ref.
tetraperoxo	1	$(\text{NH}_4)_3[\text{Nb}(\text{O}_2)_4]$	[14]
	2	$(\text{gu})_3[\text{Nb}(\text{O}_2)_4]$	[14]
	3	$(\text{gu})_3[\text{Ta}(\text{O}_2)_4]$	[17]
triperoxo	4	$\text{K}_3[\text{Nb}(\text{O}_2)_3(\text{ox})]$	[22]
	5	$\text{K}_3[\text{Nb}(\text{O}_2)_3(\text{o-phen})]$	[27]
	6	$\text{K}_3[\text{Ta}(\text{O}_2)_3(\text{o-phen})]$	[27]
	7	$(\text{gu})_2[\text{Nb}(\text{O}_2)_3(\text{picO})]$	to be published
<i>cis</i> -diperoxo	8	$\text{K}_3[\text{Nb}(\text{O}_2)_2\text{F}_4]$	[28]
	9	$(\text{NH}_4)_3[\text{Nb}(\text{O}_2)_2(\text{ox})_2]$	[14]
	10	$(\text{gu})_5[\text{Nb}_2(\text{O}_2)_4(\text{Htart})(\text{tart})] \cdot 4\text{H}_2\text{O}$	[18]
	11	$(\text{gu})_3[\text{Nb}(\text{O}_2)_2(\text{edtaO}_2)] \cdot 2\text{H}_2\text{O}$	[16]
	12	$(\text{gu})_3[\text{Ta}(\text{O}_2)_2(\text{edtaO}_2)] \cdot 2\text{H}_2\text{O}$	[17]

Tables 2–6 present the theoretical results obtained for each of the five species considered and compare them to the experimental results from IR and Raman spectroscopy reported in the literature or obtained in the present work. These tables list, for each normal mode, its corresponding vibrational motion, its activity in IR and/or Raman (R), its

calculated frequency (in cm^{-1}) and finally its frequency (in cm^{-1}) observed experimentally on the spectra.

In the tetraperoxometallate anion, the stretching vibrations of the peroxo groups, $\nu(\text{O}-\text{O})$, belong to the A_1 , B_2 and E modes. The first one is only Raman active and is due to the total symmetric vibration where all four peroxo groups vibrate in phase. The second one is only IR active, while the third one is active in IR as well as in Raman. These theoretical results are in agreement with the experimental IR and Raman spectra of complexes **1–3**, which each display two $\nu(\text{O}-\text{O})$ bands beyond 800 cm^{-1} (see Table 2). Haeuseler et al. have observed only one $\nu(\text{O}-\text{O})$ band in the IR spectrum of corresponding tantalum compounds with several counterions. This band was attributed to the $\nu(\text{O}-\text{O})$ belonging to the E mode. As far as the metal–peroxo stretching $\nu[\text{M}(\text{O}_2)]$ vibrations are concerned, two modes occur and correspond to E and A_1 species; the first one is active in both techniques while the second one is only Raman active. These bands are observed near 550 and 530 cm^{-1} , respectively, in the experimental spectra of complexes **1–3** (see Table 2).

Table 2. Theoretical results for the tetraperoxo species $[\text{M}(\text{O}_2)_4]^{3-}$ compared to the experimental results for compounds **1–3**.

Schematic representation of the normal mode	Activity	Calculated frequency ^[a] [cm^{-1}]	Observed frequency [cm^{-1}]		
			1	2	3
A_1 	IR	886	849	849	840
	R ✓				
B_2 	IR ✓	860	818	825	817
	R				
$E^{[b]}$ 	IR ✓	861	813	818	810
	R ✓				
$E^{[b]}$ 	IR ✓	502	540	554	551
	R ✓				
A_1 	IR	483	520	527	536
	R ✓				

[a] The theoretical frequencies obtained at the B3LYP/6-31+G(d) level cannot be directly compared to the experimental ones but must be scaled by some empirical factor. [b] Doubly degenerate vibrational mode.

In the case of the heteroleptic tri- and *cis*-diperoxo complexes, the theoretical results confirmed the empirical rule which states that the presence of two or three $\nu(\text{O}-\text{O})$ bands in the IR spectrum indicates the formation of a diperoxo or triperoxo complex, respectively.^[22] Moreover, according to

the theoretical results obtained, the same rule can be applied in the case of Raman spectroscopy.

The triperoxo species $[\text{M}(\text{O}_2)_3\text{L}_2]^{x-}$ shows three vibration modes which involve the $\text{O}-\text{O}$ stretching and which are all active in both IR and Raman spectroscopy. This result is in agreement with the experimental spectra illustrated in Figure 3 in the case of $(\text{gu})_2[\text{Nb}(\text{O}_2)_3(\text{picO})]$ (**7**), which each display three $\nu(\text{O}-\text{O})$ bands near 850 cm^{-1} . The additional bands occurring in the IR spectrum of compound **7** in that zone (871 and 811 cm^{-1}) are due to the bending vibration of the *N*-oxide group, $\delta(\text{N}-\text{O})$, present in the picolino ligand. The triperoxo complex also shows two $\nu[\text{M}(\text{O}_2)]$ vibrations which are both IR and Raman active, as confirmed by the experimental observations (see Figure 2). As illustrated in Table 3, the first $\nu[\text{M}(\text{O}_2)]$ mode implies the presence of two peroxo ligands, while the second one implies the presence of only one.

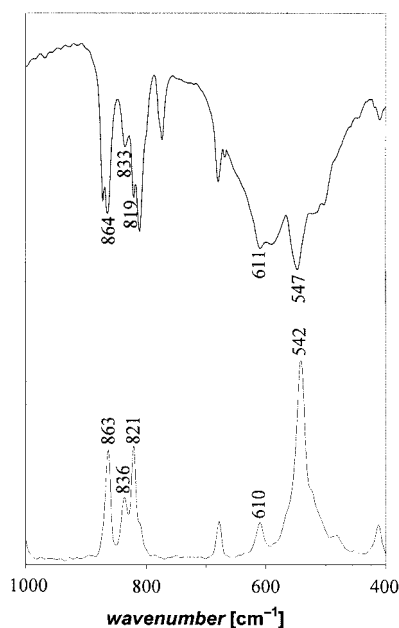
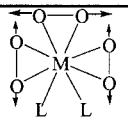
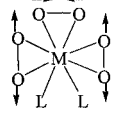
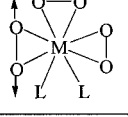
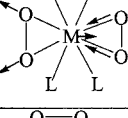
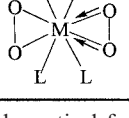


Figure 3. Experimental IR (top) and Raman (bottom) spectra of $(\text{gu})_2[\text{Nb}(\text{O}_2)_3(\text{picO})]$ (**7**).

As far as the *cis*-diperoxo species $[\text{M}(\text{O}_2)_2\text{L}_4]^{y-}$ is concerned, the theoretical calculations provide two $\nu(\text{O}-\text{O})$ vibrations. As shown in Table 4, in the first mode, of B_1 symmetry, the peroxo ligands vibrate out of phase, while in the second one, of symmetry A_1 , they vibrate in phase. The diperoxo complex also displays two $\nu[\text{M}(\text{O}_2)]$ vibrations, which are both active in IR and Raman spectroscopy. The theoretical results are in agreement with the experimental ones, which are illustrated in Figure 4 in the case of $(\text{NH}_4)_3[\text{Nb}(\text{O}_2)_2(\text{ox})_2]$ (**9**).

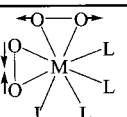
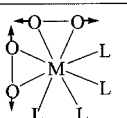
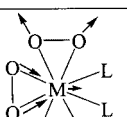
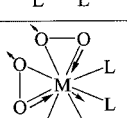
As illustrated in Table 5, the *trans*-diperoxo model compound shows two peroxo stretching modes. The antisymmetric mode is active in both IR and Raman spectroscopy while the symmetric one is only Raman active. This species also displays four metal–peroxo stretching vibrations, $\nu[\text{M}(\text{O}_2)]$, which belong to the B_1 , B_3 , B_2 and A modes, respectively. Only the first and third ones show a fair ac-

Table 3. Theoretical results for the triperoxo species $[M(O_2)_3L_2]^{x-}$ compared to the experimental results for compounds 4–7.

Schematic representation of the normal mode	Activity	Calculated frequency ^[a] [cm ⁻¹]	Observed frequency [cm ⁻¹]			
			4	5	6	7
	IR	911	852	865	865	864
	R		— ^[b]	—	—	863
	IR	884	834	815	805	833
	R		—	—	—	836
	IR	881	825	800	795	819
	R		—	—	—	821
	IR	567	568	—	—	603
	R		—	—	—	611
	IR	559	513	—	—	547
	R		—	—	—	542

[a] The theoretical frequencies obtained at the B3LYP/6-31+G(d) level cannot be directly compared to the experimental ones but must be scaled by some empirical factor. [b] Unreported value.

Table 4. Theoretical results realised for the *cis*-diperoxo species $[M(O_2)_2L_4]^{y-}$ compared to the experimental results for compounds 8–12.

Schematic representation of the normal mode	Activity	Calculated frequency ^[a] [cm ⁻¹]	Observed frequency [cm ⁻¹]					
			8	9	10	11	12	
	IR	905	880	874	866	872	873	
	R		— ^[b]	871	868	873	875	
	IR	895	860	851	850	857	857	
	R		—	850	851	854	861	
	IR	583	550	570	571	642	643	
	R		—	573	570	638	636	
	IR	542	500	537	536	554	544	
	R		—	532	531	559	555	

[a] The theoretical frequencies obtained at the B3LYP/6-31+G(d) level cannot be directly compared to the experimental ones but must be scaled by some empirical factor. [b] Unreported value.

tivity in IR spectroscopy, while the A mode is Raman active. No comparison can be made in this case with experimental data because such complexes have not been described in the literature so far.

Finally, in the case of the monoperoxo species $[M(O_2)L_6]^{z-}$, the results are quite simple because only one $\nu(O-O)$ mode and two $\nu[M(O_2)]$ vibrations – the symmetric and antisymmetric ones – are obtained (see Table 6). These three vibrational modes are all active in IR and Raman spectroscopy. Here also no comparison with the literature can be made because such compounds with an eightfold coordination are not yet known.

Conclusions

Theoretical interpretations of the experimental observations made by vibrational IR and Raman spectroscopy on eight-coordinate peroxo complexes of niobium(v) and tantalum(v) have been carried out. This study provides the normal modes of vibrations involving peroxo ligands, their corresponding calculated frequency and their activity in IR and/or Raman spectroscopy. This work thus validates the empirical rules mentioned so far for the interpretation of the vibrational spectra of eight-coordinate heteroleptic peroxo complexes, and provides important tools to develop the

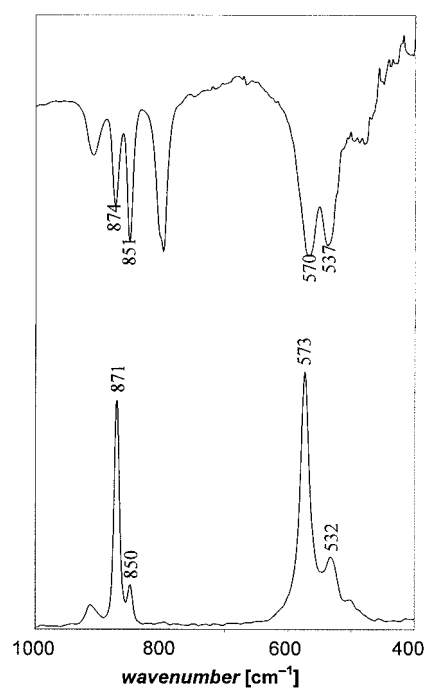
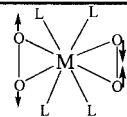
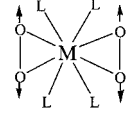
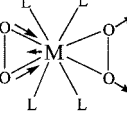
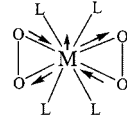
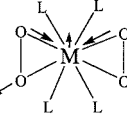
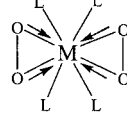
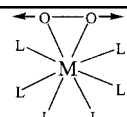
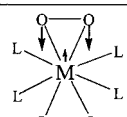
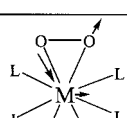
Figure 4. Experimental IR (top) and Raman (bottom) spectra of $(NH_4)_3[Nb(O_2)_2(ox)_2]$ (9).

Table 5. Theoretical results obtained for the *trans*-diperoxo species $[M(O_2)_2L_4]^{p-}$.

Schematic representation of the normal mode	Activity	Calculated frequency [cm ⁻¹]
	IR	948
	R	
	IR	947
	R	
	IR	588
	R	
	IR	568
	R	
	IR	566
	R	
	IR	523
	R	

[a] The theoretical computation gives a very small IR activity.

Table 6. Theoretical results for the monoperoxo species $[M(O_2)L_6]^{p-}$.

Schematic representation of the normal mode	Activity	Calculated frequency [cm ⁻¹]
	IR	937
	R	
	IR	598
	R	
	IR	481
	R	

coordination chemistry of peroxo species as it could be extended to equivalent complexes of other transition metals.

Experimental Section

General: The Nb^V and Ta^V complexes **1–3** and **9–12** (see Table 1) were prepared according to procedures described elsewhere.^[14,16–18] The IR spectrum of compound **7** was recorded with an FTS-135 Bio-RAD spectrometer, using KBr pellets containing ca. 1 wt.-% of the powder. FT-Raman spectra of complexes **1–3**, **7** and **9–12** were recorded with a Bruker spectrometer (type RFS100/S) at a wavelength of 1064 nm. Measurements were carried out on powders sampled on an aluminium support.

Computational Details: Theoretical calculations were performed at the Hartree–Fock and DFT levels for five stoichiometric models corresponding to tetra-, tri-, di- and monoperoxo species, of general formula $[M(O_2)_4]^{3-}$, $[M(O_2)_3L_2]^{x-}$, *cis*- and *trans*- $[M(O_2)_2L_4]^{p-}$ and $[M(O_2)L_6]^{p-}$, respectively. The metal, M, chosen for the simulation is niobium(v) and L corresponds to the oxygen atoms of oxalate, which mimic a coordinated atom from one or several mono- or polydentate ligand(s). For the central metal atom, an effective core potential was used to represent all but the valence *nd* and (*n*+1)*s* and outer core *ns* and *np* electrons. The latter were described with a double-zeta basis set, this combination being referred to as the LANL2DZ basis set. In order to check the functional dependence of the obtained results, the computations were completed using Becke's three-parameter hybrid functional (B3LYP), the Perdew 86 functional (P86) and finally the Perdew–Burke–Ernzerhof (PBE) hybrid functional. These anionic complexes require fairly good basis sets to obtain reliable results. In particular, polarisation functions are needed on the ligands to introduce enough flexibility into the wave function. The introduction of diffuse orbitals also improves the long-range spatial distribution required by the presence of negative charges. To check this point, we used two basis sets to represent the non-metal atoms, namely, the standard 6-31G(d) basis as starting point, completed afterwards by 6-31+G(d), which introduces diffuse functions on each atom. These basis sets are those available in the Gaussian series of programs.^[29] Concerning the geometry optimisation, trial structures of the selected species were taken from available crystallographic data to yield the starting points for full optimisation. All structures were optimised without any symmetry constraints and the point group was deduced from the optimised geometries. A single minimum was obtained for all *n* values except when *n* equals two, where two minima appear. Within numerical precision, the symmetry deduced for the various compounds $[M(O_2)_4]^{3-}$, $[M(O_2)_3L_2]^{x-}$, *cis*- or *trans*- $[M(O_2)_2L_4]^{p-}$ and $[M(O_2)L_6]^{p-}$ is *D*_{2d}, *C*_s, *C*_{2v} or *D*₂ and *C*₁, respectively, regardless of the method or basis set being used. These structures are, of course, “gas-phase” structures that do not consider the nature of the counterion or the incidence of the solid-state environment. We report the relative stabilities obtained for the diperoxo species in Table 7. While B3LYP gives no significant energy difference between both structures, Hartree–Fock results give a *C*_{2v} symmetry (*cis* configuration) that is some 27 kJ mol⁻¹ more stable than the *D*₂ symmetry (*trans* configuration). Finally, the P86 and PBE functional favour the *D*₂ structure slightly. A normal mode analysis was realised at the harmonic level for each obtained structure in order to obtain vibrational frequencies and to identify the normal modes involving the peroxo functions. At this level of methodology, the theoretical frequencies cannot be directly compared to the experimental ones but must be scaled by an empirical factor. As it is not useful to give all the results here, Table 8 gives an example of

the wavenumbers obtained for $[M(O_2)_3L_2]^{3-}$ at all levels of methodology. They show that the numbers obtained at the B3LYP and P86 levels are close to the experimental values and that even though a slight improvement is obtained with the diffuse basis set, it is not really significant. Hartree–Fock results, as is well known, are overestimated by some 20%, but the PBE functional does not behave very well as it overestimates the frequencies by about 10%. As the best fit was obtained with the B3LYP and P86 functionals using the diffuse basis functions, the data referred to in the above discussion are those obtained at the B3LYP level. The optimised XYZ coordinates of the niobium complexes are given in the Supporting Information (see footnote on the first page of this article). The reported data contain the DFT/B3LYP level results obtained with a LANL2DZ pseudopotential for Nb and the 6-31+G(d) basis sets for C and O atoms.

Table 7. Relative stability [kJ mol^{-1}] between *cis*- and *trans*- $[M(O_2)_2L_4]^{3-}$.

Method	6-31G(d)	With diffuse functions
B3LYP	0.3	−3.7
P86	−12.0	−16.1
PBE	−6.0	−13.6
HF	27.0	27.0

Table 8. Comparison between a selected experimental and various theoretically^[a] obtained wavenumbers of $[M(O_2)_3L_2]^{3-}$ [cm^{-1}].

Exp	B3LYP	P86	PBE	HF
513	551 (553)	525 (534)	567 (572)	641 (634)
568	559 (568)	535 (544)	579 (583)	642 (644)
825	881 (900)	844 (863)	931 (947)	1015 (1025)
834	884 (902)	845 (864)	933 (948)	1024 (1032)
852	911 (928)	870 (888)	959 (974)	1053 (1061)

[a] 6-31+G(d) and 6-31G(d) (in parentheses) basis sets.

Acknowledgments

The authors thank the Belgian National Fund for Scientific Research (FNRS) for the research fellowship allotted to D. B. and financial support.

- [1] V. Conte, F. DiFuria, S. Moro, *J. Phys. Org. Chem.* **1996**, *9*, 329–336.
- [2] K. A. Jorgensen, *Chem. Rev.* **1989**, *89*, 431–458.
- [3] R. Noyori, M. Aoki, K. Sato, *Chem. Commun.* **2003**, *16*, 1977–1986.
- [4] R. A. Sheldon, *Top. Curr. Chem.* **1993**, *164*, 21–43.
- [5] R. A. Sheldon, I. W. C. E. Arends, A. Dijkman, *Catal. Today* **2000**, *57*, 157–166.
- [6] D. C. Crans, J. J. Smee, E. Gaidamauskas, L. Q. Yang, *Chem. Rev.* **2004**, *104*, 849–902.
- [7] K. H. Thompson, J. H. McNeill, C. Orvig, *Chem. Rev.* **1999**, *99*, 2561–2571.
- [8] H. Ichinose, M. Taira, S. Furuta, H. Katsuki, *J. Am. Ceram. Soc.* **2003**, *86*, 1605–1608.
- [9] V. T. Kalinnikov, O. G. Gromov, G. B. Kunshina, A. P. Kuz'min, E. P. Lokshin, V. I. Ivanenko, *Inorg. Mater.* **2004**, *40*, 411–414.
- [10] Y. Narendar, G. L. Messing, *Chem. Mater.* **1997**, *9*, 580–587.
- [11] N. Uekawa, T. Kudo, F. Mori, Y. J. Wu, K. Kakegawa, *J. Colloid Interface Sci.* **2003**, *264*, 378–384.
- [12] Y. Yoshikawa, K. Uchino, *J. Am. Ceram. Soc.* **1996**, *79*, 2417–2421.
- [13] Y. F. Gao, Y. Masuda, H. Ohta, K. Koumoto, *Chem. Mater.* **2004**, *16*, 2615–2622.
- [14] D. Bayot, B. Tinant, M. Devillers, *Catal. Today* **2003**, *78*, 439–447.
- [15] D. Bayot, M. Devillers, *Chem. Mater.* **2004**, *16*, 5401–5407.
- [16] D. Bayot, B. Tinant, B. Mathieu, J. P. Declercq, M. Devillers, *Eur. J. Inorg. Chem.* **2003**, 737–743.
- [17] D. Bayot, B. Tinant, M. Devillers, *Inorg. Chem.* **2004**, *43*, 5999–6005.
- [18] D. Bayot, B. Tinant, M. Devillers, *Inorg. Chem.* **2005**, *44*, 1554–1562.
- [19] G. Mathern, R. Weiss, *Acta Crystallogr. Sect. B* **1971**, *27*, 1598–1609.
- [20] G. Mathern, R. Weiss, *Acta Crystallogr. Sect. B* **1971**, *27*, 1572–1581.
- [21] G. Mathern, R. Weiss, *Acta Crystallogr. Sect. B* **1971**, *27*, 1582–1597.
- [22] R. N. Shchelokov, E. N. Traggeim, M. A. Michnik, K. I. Petrov, *Russ. J. Inorg. Chem.* **1972**, *17*, 1270–1272.
- [23] A. C. Dengel, W. P. Griffith, *Polyhedron* **1989**, *8*, 1371–1377.
- [24] K. I. Selezneva, L. A. Nisels'ov, *Russ. J. Inorg. Chem.* **1968**, *13*, 45–47.
- [25] R. N. Shchelokov, E. N. Traggeim, M. A. Michnik, *Russ. J. Inorg. Chem.* **1971**, *16*, 211–213.
- [26] G. Haxhillazi, H. Haeuseler, *J. Solid State Chem.* **2004**, *177*, 3045–3051.
- [27] C. Djordjevic, N. Vuletic, *Inorg. Chem.* **1968**, *7*, 1864–1868.
- [28] N. Vuletic, C. Djordjevic, *J. Less-Common Met.* **1976**, *45*, 85–89.
- [29] M. J. Frisch, G. W. Trucks, H. B. Schlegel, G. E. Scuseria, M. A. Robb, J. R. Cheeseman, V. G. Zakrzewski, J. A. Montgomery, Jr., R. E. Stratmann, J. C. Burant, S. Dapprich, J. M. Millam, A. D. Daniels, K. N. Kudin, M. C. Strain, O. Farkas, J. Tomasi, V. Barone, M. Cossi, R. Cammi, B. Mennucci, C. Pomelli, C. Adamo, S. Clifford, J. Ochterski, G. A. Petersson, P. Y. Ayala, Q. Cui, K. Morokuma, D. K. Malick, A. D. Rabuck, K. Raghavachari, J. B. Foresman, J. Cioslowski, J. V. Ortiz, A. G. Baboul, B. B. Stefanov, G. Liu, A. Liashenko, P. Piskorz, I. Komaromi, R. Gomperts, R. L. Martin, D. J. Fox, T. Keith, M. A. Al-Laham, C. Y. Peng, A. Nanayakkara, C. Gonzalez, M. Challacombe, P. M. W. Gill, B. Johnson, W. Chen, M. W. Wong, J. L. Andres, C. Gonzalez, M. Head-Gordon, E. S. Replogle, J. A. Pople, *Gaussian 98*, revision A.7, Gaussian, Inc., Pittsburgh PA, 1998.

Received: May 11, 2005

Published Online: September 5, 2005